Int J Solids Structures Vol 15, pp 441–456
© Pergamon Press Ltd. 1979 Printed in Great Britain
0020-7683/79/0601-0441/$02.00/0

CREEP BUCKLING OF RECTANGULAR PLATES UNDER AXIAL COMPRESSION

VIGGO TVERGAARD
Department of Solid Mechanics, The Technical University of Denmark, Lyngby, Denmark

(*Received* 30 *August* 1978; *in revised form* 28 *November* 1978)

Abstract—The creep buckling behaviour is investigated for simply supported rectangular plates under axial compression. In addition to creep also elastic and plastic deformations are accounted for. The initial creep buckling behaviour at small deflections is analysed by a perturbation method, and this solution is used to obtain a simple, rough estimate of the life time. Numerical solutions for the plate creep buckling are obtained by an iterative incremental method. Based on these results the effect of the creep exponent and various effects of plasticity are discussed. The failure times obtained numerically are compared with the time estimates based on asymptotic theory and with critical times predicted in earlier investigations.

1 INTRODUCTION

Creep buckling is a type of structural failure that may occur, if the material undergoes time-dependent deformations even when the stress-state remains constant. For structural metals such creep is only observed at high temperatures, whereas for certain polymer materials creep may also occur at room temperature.

The creep buckling phenomenon has been discussed in detail by Hoff[1, 2], with special emphasis on the behaviour of plates and shells. Particularly the creep buckling behaviour of circular cylindrical shells under various loadings has been thoroughly investigated by Samuelson[3]. The buckling process is initiated by small geometrical imperfections, which are unavoidable in practice. Due to creep these initial imperfections grow and change their shape, until structural failure occurs at a certain critical time. Thus, creep buckling is not a stability problem in the classical sense, but rather a question of determining how long time it takes, before failure occurs.

The criterion of creep buckling failure used in many analyses relies on the prediction of infinite deflections at a finite critical time. However, for a column subject to elastic and creep deformations Życzkowski[4] has shown that the deflections remain finite, when large rotations are accounted for in the theory. This is also directly understandable, as deflections larger than the maximum length of the structure could never be expected. Alternatively, the criterion of creep buckling may be defined as the occurrence of infinite deflection rates at a finite time. With this criterion Huang[5] has shown that creep buckling may occur even in a large rotation model of a column, provided that plastic deformations are accounted for. However, also when the deflection rates remain finite, the structure is destroyed by creep buckling, as for a pin-ended column where even the extreme situation that the two loaded ends coincide will occur in a finite time. Estimates of life time in such cases have been discussed by various authors, and among the suggested criteria are limits on allowable deflections or on allowable strains. A criterion can also be based on creep rupture due to tensile stresses that develop during buckling[6].

An entirely different approach to creep buckling is that proposed by Rabotnov and Shesterikov[7]. Here initially perfect columns or plates are said to be stable if the dynamic response to a small disturbance is a decaying deflection. Although inertia terms are included in the linearized equations, the stability criterion relies only on the quasi static terms. One particular result is that columns subject to steady creep are never stable according to this criterion, and even if strain hardening creep is accounted for, the critical time predicted this way is usually far smaller than the useful life time of the real structure[1].

The present paper considers the creep buckling behaviour of rectangular, simply supported plates under axial compression. This problem has been studied intensively by Hoff *et al.*[8, 9], who have used an approximate analysis to obtain a closed form solution for the critical time, at which infinite deflections are predicted. An extension of this method has been used by Levi and Hoff[10] to analyse plates, for which the loaded edges are constrained to remain straight. In this

case infinite deflections are not found at a finite time, but it is found that the deflection rates increase considerably around the critical time predicted in [8]. The first investigations [8, 9] consider both creep and elastic deformations, whereas in [10] only creep is accounted for Experimental investigations [11, 12] have been made for long, simply supported plate strips under axial compression, in which the wave length of the buckling pattern that develops eventually depends on the shape of the initial imperfections and on the growth rate corresponding to various wave lengths.

In the analyses to be made here both elastic, plastic and creep deformations are accounted for. Von Kármán plate theory is used, so that the results are restricted to moderate rotations. The problem is first approached by a perturbation solution in order to study the initial creep buckling behaviour. Subsequently, the problem is analysed numerically by an incremental method based on Newton–Raphson iterations and finite element approximations. The results are used to study the effects of different creep exponents, of different levels of yield stress relative to the applied stress, and of high hardening plastic behaviour vs low hardening plastic behaviour. The results are discussed in relation to the well known post buckling behaviour of elastic plates and of elastic–plastic plates.

2. PROBLEM FORMULATION

The rectangular plates considered have the length a in the x_1 direction, the width b in the x_2 direction, and the thickness h (Fig. 1). The displacements of the plate middle surface are v_α in the directions of the in-plane Cartesian coordinates x_α, and w in the x_3 direction. The plate behaviour shall be investigated within the context of von Kármán plate theory, in which the membrane strain tensor $\epsilon_{\alpha\beta}$ and the bending strain tensor $\kappa_{\alpha\beta}$ are

$$\epsilon_{\alpha\beta} = \tfrac{1}{2}(v_{\alpha,\beta} + v_{\beta,\alpha}) + \tfrac{1}{2} w_{,\alpha} w_{,\beta} \tag{2.1}$$

$$\kappa_{\alpha\beta} = w_{,\alpha\beta} \tag{2.2}$$

and the Lagrangian strain tensor at distance x_3 from the middle surface is approximated by

$$\eta_{\alpha\beta} = \epsilon_{\alpha\beta} - x_3 \kappa_{\alpha\beta}. \tag{2.3}$$

Here, $(\ )_{,\alpha}$ denotes partial differentiation with respect to the in-plane Cartesian coordinates x_α.

The creep behaviour of the material is taken to be steady creep as described by the generalized Norton's law [13]

$$\dot{\eta}_{ij}^{C} = \tfrac{3}{2} k \sigma_e^{n-1} s_{ij}. \tag{2.4}$$

Here, the constants k and n are temperature-dependent material parameters, the stress deviator s_{ij} and the effective stress σ_e are

$$s_{ij} = \sigma_{ij} - \tfrac{1}{3}\delta_{ij}\sigma_{kk}, \quad \sigma_e = \{\tfrac{3}{2} s_{ij} s_{ij}\}^{1/2} \tag{2.5}$$

δ_{ij} is the Kronecker delta, and $(\dot{})$ denotes differentiation with respect to time. Latin indices range from 1 to 3, while Greek indices range from 1 to 2.

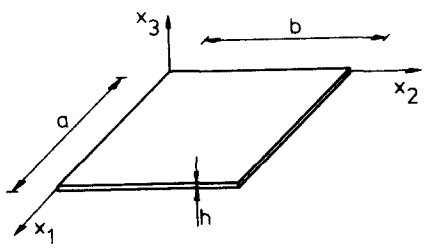

Fig. 1. Rectangular plate.

In addition to creep also elasticity and time-independent plasticity are considered. The elastic strains are given by

$$\eta_{ij}^{E} = \frac{1}{E}\{(1+\nu)\delta_{ik}\delta_{jl} - \nu\delta_{ij}\delta_{kl}\}\sigma_{kl} \tag{2.6}$$

where E and ν are Young's modulus and Poisson's ratio, respectively. The theory of plasticity employed is J_2-flow theory with isotropic hardening, in which the increment of plastic strains is given by

$$\overset{*}{\eta}_{ij}^{P} = \alpha\frac{3}{2}\left(\frac{1}{E_t} - \frac{1}{E}\right)\frac{\overset{*}{\sigma}_e}{\sigma_e}s_{ij} \tag{2.7}$$

$$\alpha = \begin{cases} 1, & \text{for } \sigma_e = (\sigma_e)_{\max} \text{ and } \overset{*}{\sigma}_e > 0 \\ 0, & \text{for } \sigma_e < (\sigma_e)_{\max} \text{ or } \overset{*}{\sigma}_e < 0 \end{cases}. \tag{2.8}$$

Here, $(^*)$ denotes differentiation with respect to some monotonically increasing parameter that characterizes the loading history. In particular, during creep under constant load time is a convenient choice for this monotonically increasing parameter. The initial value of $(\sigma_e)_{\max}$ is the yield stress σ_y, and E_t is the slope of the uniaxial stress-strain curve at the stress level σ_e. The uniaxial stress-strain behaviour is represented as a piecewise power-law with continuous tangent modulus

$$\epsilon = \begin{cases} \dfrac{\sigma}{E}, & \text{for } \sigma < \sigma_y \\ \dfrac{\sigma_y}{E}\left[\dfrac{1}{m}\left(\dfrac{\sigma}{\sigma_y}\right)^m - \dfrac{1}{m} + 1\right], & \text{for } \sigma \geq \sigma_y \end{cases} \tag{2.9}$$

where m is the strain hardening exponent.

The total strain is taken to be the sum of the elastic, plastic and creep strains

$$\eta_{ij} = \eta_{ij}^{E} + \eta_{ij}^{P} + \eta_{ij}^{C} \tag{2.10}$$

as given by (2.4), (2.6) and (2.7). Thus, in the present paper creep and plasticity are taken to be independent processes, and the interaction between them is neglected.

The sum of (2.7) and the incremental form of (2.6) can be inverted to express the stress increments in terms of the time-independent strain increments

$$\overset{*}{\sigma}_{ij} = L_{ijkl}(\overset{*}{\eta}_{kl}^{E} + \overset{*}{\eta}_{kl}^{P}) \tag{2.11}$$

where the instantaneous moduli are

$$L_{ijkl} = \frac{E}{1+\nu}\left\{\frac{1}{2}(\delta_{ik}\delta_{jl} + \delta_{il}\delta_{jk}) + \frac{\nu}{1-2\nu}\delta_{ij}\delta_{kl} - \alpha\frac{3}{2}\frac{E/E_t - 1}{E/E_t - (1-2\nu)/3}\frac{s_{ij}s_{kl}}{\sigma_e^2}\right\}. \tag{2.12}$$

As the stress state in the plate is approximately plane, only the in-plane stresses enter into the constitutive relations. Thus, using (2.4), (2.10) and the usual assumption $\eta_{\alpha 3} = 0$ for plates the relation (2.11) can be written as

$$\overset{*}{\sigma}_{\alpha\beta} = \hat{L}_{\alpha\beta\gamma\delta}(\overset{*}{\eta}_{\gamma\delta}^{E} + \overset{*}{\eta}_{\gamma\delta}^{P}) \tag{2.13}$$

where the in-plane moduli are given by

$$\hat{L}_{\alpha\beta\gamma\delta} = L_{\alpha\beta\gamma\delta} - \frac{L_{\alpha\beta 33}L_{\gamma\delta 33}}{L_{3333}}. \tag{2.14}$$

The membrane stress tensor $N_{\alpha\beta}$ and the moment tensor $M_{\alpha\beta}$ are taken to be

$$N_{\alpha\beta} = \int_{-h/2}^{h/2} \sigma_{\alpha\beta}\, dx_3, \quad M_{\alpha\beta} = -\int_{-h/2}^{h/2} \sigma_{\alpha\beta} x_3\, dx_3. \tag{2.15}$$

In the numerical method to be described subsequently the requirement of equilibrium is introduced through the principle of virtual work

$$\int_A [N_{\alpha\beta}\delta\epsilon_{\alpha\beta} + M_{\alpha\beta}\delta\kappa_{\alpha\beta}]\, dA = \delta W \tag{2.16}$$

where δW is the external virtual work and A is the area of the plate.

The plates are here taken to be simply supported at all four edges

$$\begin{aligned} &w = 0, \quad M_{11} = 0 \quad \text{at} \quad x_1 = 0, a \\ &w = 0, \quad M_{22} = 0 \quad \text{at} \quad x_2 = 0, b. \end{aligned} \tag{2.17}$$

Two different sets of in-plane boundary conditions are considered. In a few cases the edges are taken to be unconstrained with

$$N_{12} = 0 \quad \text{at} \quad x_1 = 0, a \quad \text{and} \quad x_2 = 0, b \tag{2.18}$$

$$N_{22} = 0 \quad \text{at} \quad x_2 = 0, b \tag{2.19}$$

$$N_{11} = \lambda\sigma_{11}^I h \quad \text{at} \quad x_1 = 0, a \tag{2.20}$$

where λ is a positive load parameter, and σ_{11}^I is a constant. In the other cases the loaded edges are required to remain straight, so that (2.18–2.19) are still valid, but (2.20) is replaced by

$$v_1(0, x_2) = -v_1(a, x_2) = U \tag{2.21}$$

where the constant U is determined by the condition

$$\int_0^b N_{11}\, dx_2 = \lambda\sigma_{11}^I hb \quad \text{at} \quad x_1 = 0, a. \tag{2.22}$$

The conditions (2.21) and (2.22) also represent the behaviour of a long simply supported plate strip under axial compression, where b is the width and a is the half wavelength of a buckling pattern in the axial direction.

For both sets of boundary conditions the stress state in a perfect plate prior to bifurcation consists of a constant uniaxial compressive stress $\sigma_{11} = \lambda\sigma_{11}^I$ at every point of the plate. The bifurcation mode is of the form

$$\overset{(1)}{w} = h \sin\frac{\pi x_1}{a} \sin\frac{\pi x_2}{b} \tag{2.23}$$

and the corresponding value of the critical load parameter for bifurcation in the elastic range is

$$\lambda_E = -\frac{1}{\sigma_{11}^I}\left(\frac{\pi}{b}\right)^2 \frac{Eh^2}{12(1-\nu^2)}\left(\frac{b}{a} + \frac{a}{b}\right)^2. \tag{2.24}$$

For bifurcation in the plastic range the critical load parameter is

$$\lambda_P = -\frac{1}{\sigma_{11}^I h}\left(\frac{\pi}{b}\right)^2 \left[D_1\left(\frac{b}{a}\right)^2 + 2(D_{12} + D_G) + D_2\left(\frac{a}{b}\right)^2\right] \tag{2.25}$$

where $D_1 = \hat{L}_{1111}h^3/12$, $D_2 = \hat{L}_{2222}h^3/12$, $D_{12} = \hat{L}_{1122}h^3/12$, $D_G = \hat{L}_{1212}h^3/6$, and $\hat{L}_{\alpha\beta\gamma\delta}$ are inserted as the instantaneous plastic moduli.

The reference load λ_R to be used in the following is chosen as the minimum elastic bifurcation load for a fixed width b, which is given by

$$\lambda_R = -\frac{1}{\sigma_{11}^I}\left(\frac{\pi}{b}\right)^2 \frac{Eh^2}{3(1-\nu^2)} \tag{2.26}$$

corresponding to the case of square buckles, $a = b$ in (2.24).

The time scale used in creep problems is often based on the time needed to reach a certain creep strain under uniaxial stress. Here, this strain is chosen as the prebuckling strain at elastic buckling of a square plate, and thus using (2.4) and (2.26) the reference time is defined as

$$t_R = \frac{\pi^2}{3(1-\nu^2)}\left(\frac{h}{b}\right)^2 \frac{1}{k|\sigma|^n} \tag{2.27}$$

where $\sigma = \lambda\sigma_{11}^I$ is the average compressive stress.

For a rectangular plate with elastic material behaviour and steady creep Hoff[1, 2, 8] and Hoff *et al.*[9] have developed a formula for the critical time t_{cr} at which the deflections tend towards infinity

$$t_{cr} = t_R C_1\left(1-\frac{\lambda}{\lambda_E}\right)\ln\left[1 + C_2\left(\frac{1-\lambda/\lambda_E}{\bar{\xi}}\right)^{n-1}\right]. \tag{2.28}$$

Here $\bar{\xi}$ is the amplitude of an initial geometrical imperfection in the shape of the bifurcation mode (2.23) and the constants are[2]

$$C_1 = 1.74/n^{1.42}, \quad C_2 = 3.08/e^{0.567n}$$
$$3 \le n \le 7. \tag{2.29}$$

The analysis leading to (2.28) is made for a sandwich model of a plate using a number of approximations. For example, the stresses in the two faces and the deflection are expanded in double trigonometric series, retaining only the first term, which means neglecting some effects of geometric nonlinearities. The analysis first carried out for $n = 3$[8] was later extended to $n = 5$ and $n = 7$[9], and these three results form the basis of the expressions (2.29).

3. PERTURBATION ANALYSIS

In this section the initial creep buckling behaviour of a plate with a small imperfection shall be investigated by a perturbation procedure. A similar procedure has been used previously for the analysis of tensile instabilities[14] and for creep buckling of a cylindrical shell under external pressure[15]. However, in [15] the approximation is made that the effective stress in (2.4) is taken to be constant through the thickness.

The analysis is first made for a material in which elastic and plastic strains are neglected. Thus, $\dot{\eta}_{ij}^C$ given by (2.4) is the total strain rate, as was also assumed in [14, 15]. The displacements, strains and stresses are written as

$$v_\alpha = v_\alpha^0 + \tilde{v}_\alpha, \quad w = w^0 + \tilde{w},$$
$$\eta_{ij} = \eta_{ij}^0 + \tilde{\eta}_{ij}, \quad \sigma_{ij} = \sigma_{ij}^0 + \tilde{\sigma}_{ij} \tag{3.1}$$

where the solution for the perfect plate at the current load level λ and time t is denoted by $(\,)^0$, while $(\tilde{\ })$ denotes small perturbation quantities, which are equal to the initial imperfection at $\lambda = 0$, $t = 0$. The geometrical imperfections considered in this analysis are taken in the shape of the bifurcation mode (2.23) with amplitude $\bar{\xi}$. All equations are linearized with respect to the small perturbation quantities. Thus, the constitutive equation (2.4) yields the linearized relation

$$\dot{\tilde{\eta}}_{ij}^C = \frac{3}{2}k(\sigma_e^0)^{n-1}\left[\tilde{s}_{ij} + (n-1)\frac{3}{2}\frac{s_{ij}^0 s_{kl}^0}{(\sigma_e^0)^2}\tilde{s}_{kl}\right]. \tag{3.2}$$

For the present case, where the only nonvanishing stress in the perfect plate is $\sigma_{11}^0 = \lambda\sigma_{11}^I = -\sigma_e^0$, the relations (3.2) take the form

$$\begin{aligned}
\dot{\tilde{\eta}}_{11}^C &= \frac{3}{2}k(\sigma_e^0)^{n-1}n\tilde{s}_{11} \\
\dot{\tilde{\eta}}_{22}^C &= \frac{3}{2}k(\sigma_e^0)^{n-1}\left[\tilde{s}_{22} - \frac{n-1}{2}\tilde{s}_{11}\right] \\
\dot{\tilde{\eta}}_{33}^C &= \frac{3}{2}k(\sigma_e^0)^{n-1}\left[\tilde{s}_{33} - \frac{n-1}{2}\tilde{s}_{11}\right] \\
\dot{\tilde{\eta}}_{12}^C &= \frac{3}{2}k(\sigma_e^0)^{n-1}\tilde{s}_{12}.
\end{aligned} \tag{3.3}$$

In the inverted form of (3.3) the plane stress condition, $\tilde{\sigma}_{33} = 0$, and the incompressibility of creep deformations are used to express $\tilde{\sigma}_{\alpha\beta}$ in terms of $\dot{\tilde{\eta}}_{\gamma\delta}^C$. Inserting this relation in (2.15) and using (2.3) the following linearized expressions for the perturbations of the membrane stress tensor and the moment tensor are obtained

$$\begin{aligned}
\tilde{N}_{11} &= \frac{2h}{3k(\sigma_e^0)^{n-1}}\left[\frac{n+3}{2n}\dot{\tilde{\epsilon}}_{11}^C + \dot{\tilde{\epsilon}}_{22}^C\right] \\
\tilde{N}_{22} &= \frac{2h}{3k(\sigma_e^0)^{n-1}}[2\dot{\tilde{\epsilon}}_{22}^C + \dot{\tilde{\epsilon}}_{11}^C] \\
\tilde{N}_{12} &= \frac{2h}{3k(\sigma_e^0)^{n-1}}\dot{\tilde{\epsilon}}_{12}^C.
\end{aligned} \tag{3.4}$$

$$\begin{aligned}
\tilde{M}_{11} &= \frac{h^3}{18k(\sigma_e^0)^{n-1}}\left[\frac{n+3}{2n}\dot{\tilde{\kappa}}_{11}^C + \dot{\tilde{\kappa}}_{22}^C\right] \\
\tilde{M}_{22} &= \frac{h^3}{18k(\sigma_e^0)^{n-1}}[2\dot{\tilde{\kappa}}_{22}^C + \dot{\tilde{\kappa}}_{11}^C] \\
\tilde{M}_{12} &= \frac{h^3}{18k(\sigma_e^0)^{n-1}}\dot{\tilde{\kappa}}_{12}^C.
\end{aligned} \tag{3.5}$$

Substituting (3.1) in (2.1)–(2.2), using $w^0 \equiv 0$, gives to lowest order

$$\begin{aligned}
\dot{\tilde{\epsilon}}_{\alpha\beta} &= \frac{1}{2}(\dot{\tilde{v}}_{\alpha,\beta} + \dot{\tilde{v}}_{\beta,\alpha}) \\
\dot{\tilde{\kappa}}_{\alpha\beta} &= \dot{\tilde{w}}_{,\alpha\beta}
\end{aligned} \tag{3.6}$$

so that the nonlinear part of (2.1) has no effect on $\tilde{\epsilon}_{\alpha\beta}$. Equilibrium is expressed by the principle of virtual work (2.16), linearized with respect to perturbation quantities, and the corresponding Euler equations are

$$-\tilde{N}_{\alpha\beta,\beta} = 0 \tag{3.7}$$

$$\tilde{M}_{\alpha\beta,\alpha\beta} - N_{\alpha\beta}^0\tilde{w}_{,\alpha\beta} = 0. \tag{3.8}$$

Using (3.4) and (3.6) it is directly seen that the inplane equilibrium equations (3.7) are solved by $\tilde{v}_\alpha \equiv 0$, $\tilde{N}_{\alpha\beta} \equiv 0$, for both sets of in-plane boundary conditions (2.18)–(2.22). Equation (3.8) with (3.5) and (3.6) substituted takes the form

$$\frac{n+3}{2n}\dot{\tilde{w}}_{,1111} + 4\dot{\tilde{w}}_{,1122} + 2\dot{\tilde{w}}_{,2222} - \frac{18k(\sigma_e^0)^{n-1}}{h^3}N_{11}^0\tilde{w}_{,11} = 0 \tag{3.9}$$

as $N_{11}^0 = \lambda\sigma_{11}^I h$ is the only nonvanishing component component of $N_{\alpha\beta}^0$. Assuming a solution

$\tilde{w} = \tilde{\xi}_w^{(1)}$ in the shape of the bifurcation mode (2.23), eqn (3.9) yields

$$\dot{\tilde{\xi}} - B\tilde{\xi} = 0 \tag{3.10}$$

$$B = -N_{11}^0 \frac{9k(\sigma_e^0)^{n-1}}{h^3}\left(\frac{b}{\pi}\right)^2 \frac{\left(\frac{a}{b}\right)^2}{\frac{n+3}{4n} + 2\left(\frac{a}{b}\right)^2 + \left(\frac{a}{b}\right)^4}. \tag{3.11}$$

With the initial condition given by the imperfection $\dot{w} = \bar{\xi}_w^{(1)}$, the solution of (3.10) for constant load level is

$$\tilde{\xi} = \bar{\xi} e^{Bt}. \tag{3.12}$$

In a long plate strip with a given width b the highest creep rate is obtained for the wave length maximizing B. This occurs for the aspect ratio

$$\frac{a}{b} = \sqrt[4]{\frac{n+3}{4n}} \tag{3.13}$$

When both elastic and creep strains are accounted for, the analysis is somewhat modified. The total strains vary linearly through the thickness according to (2.3), but the same is true separately for the elastic strains and the creep strains due to the linearity of the relations (3.3) and of Hooke's law (2.6). Thus, the membrane strain tensor $\tilde{\epsilon}_{\alpha\beta}$ and the bending strain tensor $\tilde{\kappa}_{\alpha\beta}$ each consist of an elastic part and a creep part, and in the solution assumption $\tilde{w} = \tilde{\xi}_w^{(1)}$ the amplitude may be written as the sum of an elastic and a creep part, $\tilde{\xi} = \tilde{\xi}^E + \tilde{\xi}^C$. The solution of the in-plane equation (3.7) remains zero. The moment tensor to be substituted in (3.8) may be expressed in terms of the elastic bending strain tensor

$$\tilde{M}_{\alpha\beta} = \frac{Eh^3}{12(1-\nu^2)}\{(1-\nu)\tilde{\kappa}_{\alpha\beta}^E + \nu\delta_{\alpha\beta}\tilde{\kappa}_{\gamma\gamma}^E\} \tag{3.14}$$

as well as by (3.5). Substitution of (3.14) gives

$$\tilde{\xi}^E = \tilde{\xi}^C \frac{\lambda/\lambda_E}{1-\lambda/\lambda_E} \tag{3.15}$$

valid for a load parameter $\lambda < \lambda_E$, where λ_E is given by (2.24). Substitution of (3.5) gives, instead of (3.10),

$$\dot{\tilde{\xi}}^C - B(\tilde{\xi}^C + \tilde{\xi}^E) = 0. \tag{3.16}$$

Using (3.15) and the initial imperfection amplitude $\bar{\xi}$ the solution of (3.16) in terms of the total amplitude is obtained as

$$\tilde{\xi} = \frac{\bar{\xi}}{1-\lambda/\lambda_E} e^{[B/(1-\lambda/\lambda_E)t]}. \tag{3.17}$$

The time needed to reach a certain amplitude is readily obtained from (3.17). For example, after that the load has been applied, the time t_1 needed to further increase the amplitude $\tilde{\xi}$ by unity is given by

$$t_1 = \frac{1-\lambda/\lambda_E}{B} \ln\left[1 + (1-\lambda/\lambda_E)\frac{1}{\bar{\xi}}\right]. \tag{3.18}$$

Thus, t_1 is the time it takes for the maximum deflection to grow one plate thickness after $t = 0$.

Since the perturbation analysis is only valid for small deflections, the time t_1 is a rather arbitrary measure of the rate of creep buckling. However, as most of the life time is usually spent at small deflections with a very small growth rate, and rapid growth is usually confined to a limited final stage, the expression (3.18) may give a useful indication of the structural behaviour. In section 4 the time t_1 shall be compared with numerical results.

If also plastic deformations are included, the analysis is considerably complicated by the necessity to account for the effect of elastic unloading. A reasonable approximate result may be obtained[16] on the basis of the hypoelastic theory that results from neglecting elastic unloading. Thus, the amplitude $\tilde{\xi}_H$ reached at load level λ in a hypoelastic plate may be determined by the regular perturbation procedure described in [16], and subsequently, during creep, plasticity only enters the perturbation analysis through the plastic moduli corresponding to the perfect plate at load level λ. When λ_H is the bifurcation load of an elastic orthotropic plate with moduli equal to these plastic moduli, the analysis yields (for $\lambda < \lambda_H$)

$$\tilde{\xi} = \tilde{\xi}_H \, \mathrm{e}^{[B/(1-\lambda/\lambda_H)t]}. \tag{3.19}$$

It should be noted, however, that due to the limited range of validity of the asymptotic analysis plasticity may considerably affect the actual creep buckling behaviour, without appearing in the result (3.19).

4. NUMERICAL METHOD AND RESULTS

An investigation of plate creep buckling taking full account of material and geometric nonlinearities requires a numerical analysis. Here, such an analysis shall be discussed and several results shall be presented.

4.1 *Method of analysis*

The numerical analysis of creep buckling behaviour to be used here is based on the principle of virtual work (2.16). A finite element approximation of the displacement fields is used, in which the nodal degrees of freedom are denoted by q_j. Then, according to (2.16), the nonlinear algebraic equations to be solved are

$$\begin{aligned} &F_j = 0, \quad \text{for} \quad j = 1, 2, \ldots N \\ &F_j = \int_A \left\{ N_{\alpha\beta} \frac{\partial \epsilon_{\alpha\beta}}{\partial q_j} + M_{\alpha\beta} \frac{\partial \kappa_{\alpha\beta}}{\partial q_j} \right\} \mathrm{d}A - \frac{\partial W}{\partial q_j} \end{aligned} \tag{4.1}$$

where N is the number of degrees of freedom. If an approximate solution $[q_j]_0$ is known, the exact solution may be written on the form $q_j = [q_j]_0 + \mathrm{d}q_j$. Substitution of this exact solution into (4.1) and linearization with respect to the small deviations $\mathrm{d}q_j$ leads to the following equations

$$\sum_{i=1}^{N} \left[\frac{\partial F_j}{\partial q_i} \right]_0 \mathrm{d}q_i = -[F_j]_0, \quad \text{for} \quad j = 1, 2, \ldots N. \tag{4.2}$$

Here, $[\ ]_0$ denotes the value at the approximate solution $[q_j]_0$ and the derivatives are

$$\frac{\partial F_j}{\partial q_i} = \int_A \left\{ \frac{\partial N_{\alpha\beta}}{\partial q_i} \frac{\partial \epsilon_{\alpha\beta}}{\partial q_j} + \frac{\partial M_{\alpha\beta}}{\partial q_i} \frac{\partial \kappa_{\alpha\beta}}{\partial q_j} + N_{\alpha\beta} \frac{\partial^2 \epsilon_{\alpha\beta}}{\partial q_i \partial q_j} + M_{\alpha\beta} \frac{\partial^2 \kappa_{\alpha\beta}}{\partial q_i \partial q_j} \right\} \mathrm{d}A - \frac{\partial^2 W}{\partial q_i \partial q_j} \tag{4.3}$$

in which the last term vanishes, as W depends linearly on the displacements of the loaded edges, and the last term under the integral vanishes due to the linearity of (2.2). The equations (4.2) are used in the Newton–Raphson method to iteratively improve the approximate solution.

Accounting for plasticity and creep in this solution procedure is done by an incremental method rather similar to that described by Bushnell[17]. As a start the solution $(q_j)_I$ is known at a given time and load level. Then a time increment Δt and (or) a load increment $\Delta\lambda$ are specified, and the corresponding solution increments Δq_j are determined by the Newton–Raphson iteration. Subsequently, the corresponding values of stresses and creep strains at each

integration point are adjusted by a subincrementation (to be described in the next paragraph), and then Δq_j are improved by a new Newton–Raphson iteration, etc. until the solution has finally converged. During each Newton–Raphson iteration the creep strains and the moduli $\hat{L}_{\alpha\beta\gamma\delta}$ at each integration point are kept fixed at the values found by the last subincrementation. Thus, in (4.3) the derivatives $\partial N_{\alpha\beta}/\partial q_i$ and $\partial M_{\alpha\beta}/\partial q_i$ are expressed in terms of $\partial \epsilon_{\gamma\delta}/\partial q_i$ and $\partial \kappa_{\gamma\delta}/\partial q_i$, using (2.3), (2.13) and (2.15). With the symmetry $\hat{L}_{\alpha\beta\gamma\delta} = \hat{L}_{\gamma\delta\alpha\beta}$ the stiffness matrix is symmetric in the linear equations (4.2).

After convergence of the Newton–Raphson iteration a subincrementation is performed at each integration point. The total strains at the initial solution $(q_j)_I$ are subtracted from the strains at the current solution $(q_j)_I + \Delta q_j$, to yield the difference $\Delta \eta_{\gamma\delta}$. The corresponding change of creep strains $\Delta \eta^C_{\gamma\delta}$ during the whole increment is known from the previous subincrementation. Now, the change of elastic–plastic strains is divided into M equal subincrements

$$\overset{*E}{\eta}_{\gamma\delta} + \overset{*P}{\eta}_{\gamma\delta} = (\Delta \eta_{\gamma\delta} - \Delta \eta^C_{\gamma\delta})/M \tag{4.4}$$

and the new stresses are computed by M successive applications of (2.13). At each of these M subincrements the moduli $\hat{L}_{\alpha\beta\gamma\delta}$ are computed according to the current value of the effective stress σ_e, using (2.8). Also the growth of creep strains during each subincrement is computed, using (2.4) and the time increment $\Delta t/M$, and the sum of these changes is denoted by $\Delta \eta^C_{\gamma\delta}$, to be used in the next subincrementation. As the creep rate (2.4) is strongly stress dependent, particularly for high values of the creep exponent n, the convergence is greatly improved by using underrelaxation in the iterative determination of $\Delta \eta^C_{\gamma\delta}$.

It may be mentioned here that the elastic–plastic-creep behaviour could alternatively be computed by a straightforward linear incremental procedure, based on the incremental principle of virtual work. This procedure is in fact the special case of the iterative method described above, in which (4.2) is solved only once in each increment and only one subincrement is used to update the stresses. A solution could also be based on the variational theorem developed by Sanders *et al.* [18], which is an extension of Reissner's variational theorem in elasticity.

The finite element approximation of displacement fields is made in terms of rectangular, conforming plate elements. In each element the deflections are approximated by products of Hermitian cubics in the x_1- and x_2-directions, and the four nodal parameters at each corner node are w, $w_{,1}$, $w_{,2}$ and $w_{,12}$. The same approximation is used for the in-plane displacement fields v_1 and v_2, within each element. The integrals in (4.1) and (4.3) are evaluated by 4×4 point Gaussian quadrature within each element, while the integrals (2.15) through the thickness are evaluated by a 7 point Simpson's rule.

With the initial imperfection $\bar{w} = \bar{\xi}^{(1)}_w$ in the shape of the bifurcation mode (2.23) the deflections remain symmetric about the lines $x_1 = a/2$ and $x_2 = b/2$. Therefore, symmetry conditions are prescribed along these two lines, and it is sufficient to consider only one quarter of the plate. This quarter of the plate is divided into 4 elements, 2 in each coordinate direction.

For the in-plane boundary conditions (2.21) and (2.22) a special procedure must be used in each Newton–Raphson iteration. First the eqn (4.2) are solved with the edge displacement $\mathrm{d}U = 0$ prescribed in (2.21), to yield the solution $(\mathrm{d}q_i)_1$, and secondly the solution $(\mathrm{d}q_i)_2$ is found corresponding to zero loads and prescribed edge displacement $\mathrm{d}U = 1$. Finally, a Rayleigh–Ritz procedure is used to determine the linear combination of $(\mathrm{d}q_i)_1$ and $(\mathrm{d}q_i)_2$ yielding the solution $\mathrm{d}q_i$ that solves (4.2) with the actual boundary conditions.

In the computations to be discussed here the load is applied first, at $t = 0$, and subsequently creep occurs at constant load level. The given load level is reached in one or two increments, whereas the number of time increments used is about 25. The magnitude Δt of a time increment is chosen according to an estimate of the growth of the maximum deflection during the increment, initially based on the asymptotic formula (3.17) and subsequently on the growth in previous increments. The number of subincrements (4.4) to be used may be controlled during the iteration, but here $M = 10$ has been used in each increment.

4.2 *Numerical results*

Most of the numerical results to be shown are obtained for plates with $h/b = 0.035$ and $\nu = 0.3$, at a load level $\lambda/\lambda_R = 0.65$, where the reference load λ_R is the elastic bifurcation load

for square buckles (2.26). In Figs. 2–4 the creep buckling of elastic plates is considered, whereas in Figs. 5–9 effects of plasticity are also accounted for. In these figures the growth of the maximum plate deflection w_{max} is plotted as a function of time t/t_R, where t_R is given by (2.27) and here w is taken to denote deflections in addition to the initial imperfection.

Two different criteria of creep failure shall be used here. The *failure time* t_F is taken to be reached when either

$$\frac{dw_{max}}{dt} = \infty, \quad \text{at} \quad t = t_F \tag{4.5}$$

or

$$w_{max}/h = 10, \quad \text{at} \quad t = t_F. \tag{4.6}$$

According to the first criterion (4.5) the life time is well defined, in the sense that any further creep will lead to immediate structural collapse. However, in many cases it turns out that w_{max} continues to grow monotonically with time, and after some time the structure ceases to be useful for engineering purposes. In such cases the definition of the failure time will depend on a choice of limits for usefulness, and thus differs considerably from the definition in (4.5). These

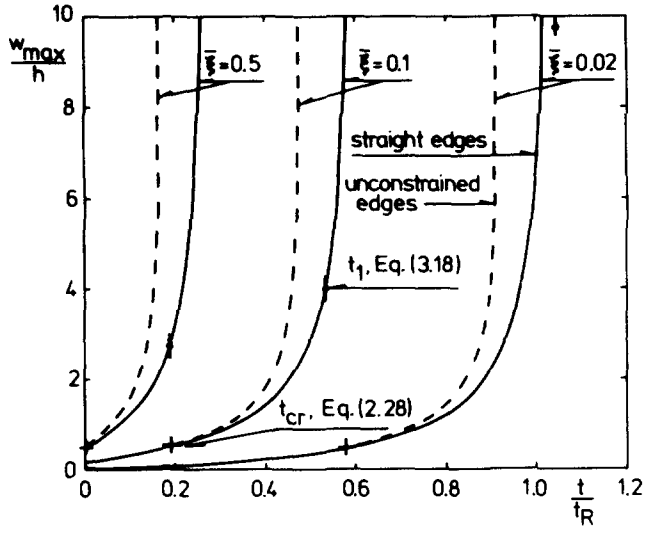

Fig. 2. Maximum deflection vs time for elastic plate subject to creep buckling ($h/b = 0.035$, $a/b = 1$, $\nu = 0.3$, $n = 6$, $\lambda/\lambda_R = 0.65$).

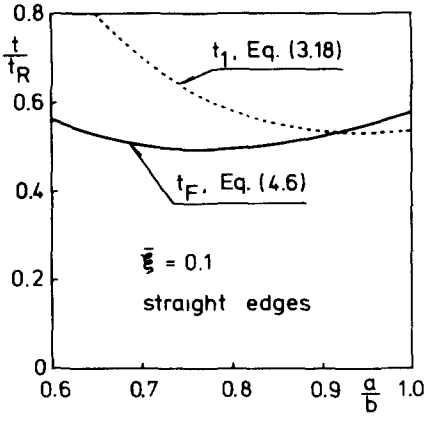

Fig. 3. Failure time vs aspect ratio for elastic plate subject to creep buckling ($h/b = 0.035$, $\nu = 0.3$, $n = 6$, $\lambda/\lambda_R = 0.65$).

limits may be defined in terms of maximum allowable deflections or strains, or in terms of some other measure of the creep process. Here, according to (4.6), a maximum allowable deflection equal to ten plate thicknesses is chosen.

Figure 2 displays results for square plates with various initial imperfection amplitudes. Here and in the following figures the solid curves refer to plates, in which the loaded edges remain straight according to (2.21) and (2.22), whereas the dashed curves refer to plates with unconstrained in-plane conditions (2.20). Initially, at small deflections, these two cases differ very little, but for larger deflections the creep rate is considerably higher in the plates with unconstrained edges. In both cases the failure time t_F, according to (4.6), is strongly imperfection-sensitive. As a comparison the critical time t_{cr} predicted by Hoff's formula (2.28) and the time t_1 based on the asymptotic theory (3.18) are also indicated in the figure for the three different imperfection amplitudes. It is noted that the time t_{cr} gives a rather conservative estimate of the failure time t_F. Particularly for the larger imperfection $\bar{\xi} = 0.5$ the ratio t_{cr}/t_F is less than 0.004, and in fact the predictions based on (2.28) seem extremely small in cases where the ratio $\bar{\xi}/(1 - \lambda/\lambda_E)$ exceeds unity. The time t_1 gives a reasonable estimate of t_F for all three imperfections in Fig. 2, but is not always conservative.

The highest rate of creep buckling according to the asymptotic solution (3.12) is obtained for a wave length $a/b = 0.78$, when $n = 6$ is substituted into (3.13). If also elastic deformations are accounted for as in (3.17), this wave length is slightly larger, due to the dependence of λ_E on a/b. In Fig. 3 the times t_F and t_1 are plotted as functions of a/b, corresponding to the imperfection $\bar{\xi} = 0.1$. Here, t_F is computed for the in-plane conditions (2.21)–(2.22) corresponding to the behaviour of a long plate strip, in which the ratio of the half wave length a to the width b may take on any value. In Fig. 3 it is seen that according to the numerical results the wavelength of the initial imperfection that grows fastest corresponds to a value of a/b close to 0.8.

In Fig. 4 a square plate is considered, which is identical with that of Fig. 2 except for the smaller creep exponent $n = 3$. Clearly, this change has a number of strong effects, one being that the imperfection-sensitivity is much reduced. Another effect is that the life time of the structure is less well defined, in the sense that the failure time t_F, at which $w_{max}/h = 10$, differs very considerably from the time at which w_{max}/h has reached for example half this value. This is particularly clear in the cases where the loaded edges are constrained to remain straight, but also for the case of unconstrained edges included in Fig. 4 the rate of growth of w_{max} is far less than found in Fig. 2. The behaviour observed in Fig. 4 is related to the well known stable post-buckling behaviour of elastic plates. As the buckling deflections grow, a redistribution of membrane stresses occurs, which reduces the rate of creep buckling, even below that predicted by the asymptotic solution (3.17). In Fig. 2 this stiffening effect is less dominant than the much

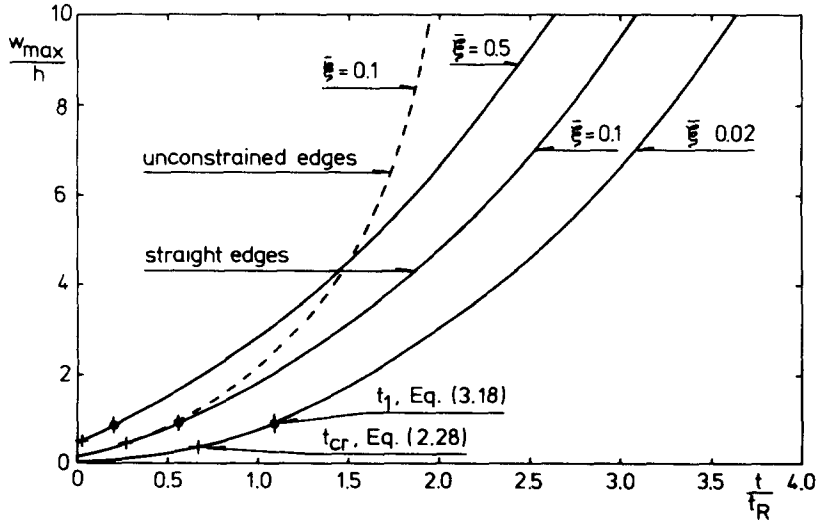

Fig. 4 Maximum deflection vs time for elastic plate subject to creep buckling ($h/b = 0.035$, $a/b = 1$, $\nu = 0.3$, $n = 3$, $\lambda/\lambda_R = 0.65$).

stronger sensitivity of the creep rate (2.4) to increases of the stresses, due to the higher creep exponent $n = 6$. Neither t_{cr} nor t_1 are very good estimates of the failure time t_F in Fig. 4, but t_1 is less conservative, particularly for the larger imperfection.

The effect of plasticity is studied in Fig. 5 for a plate otherwise identical with that of Fig. 2. The strain hardening exponent is $m = 10$, and the yield stress σ_Y is smaller than the elastic bifurcation stress, so that bifurcation of the perfect plate occurs in the plastic range with $\lambda_P/\lambda_E = 0.910$. Here creep buckling occurs for rather small deflections, by reaching an actual instability condition (4.5), at which collapse occurs instantaneously. Due to the small deflections the results differ little for the constrained and the unconstrained in-plane boundary conditions. The failure times are reduced relative to those obtained in Fig. 2 for elastic plates, and the imperfection-sensitivity is considerably increased by plasticity. In fact, for somewhat larger imperfections the failure time reduces to zero, as the corresponding maximum load carrying capacity without creep is less than the load $\lambda/\lambda_R = 0.65$ to be applied. It is noted that for the present plate the load level corresponds to $\lambda/\lambda_P = 0.714$. The maximum load carrying capacity for various imperfections has been computed in Ref. [16] for a square elastic–plastic plate with exactly the same geometry and material properties considered here. Figure 6 shows a plot of the load levels vs imperfection amplitudes, at which collapse occurs without any creep. For the constrained boundary conditions (2.21) and (2.22) the computations are new, whereas for the unconstrained edges the curve is partly based on [16]. At the same time it has been checked that the results obtained by the present iterative method agree very well with those obtained by the linear incremental method in [16].

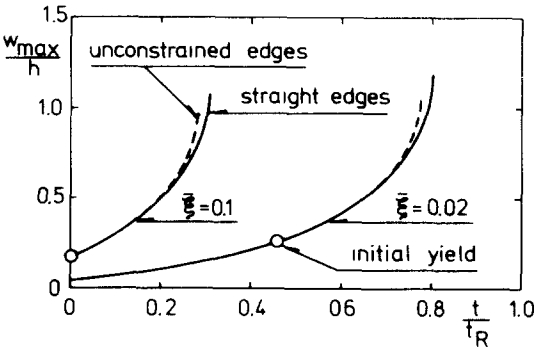

Fig. 5. Maximum deflection vs time for elastic–plastic plate subject to creep buckling ($h/b = 0.035$, $a/b = 1$, $\nu = 0.3$, $n = 6$, $\sigma_Y/E = 0.00337$, $m = 10$, $\lambda/\lambda_R = 0.65$)

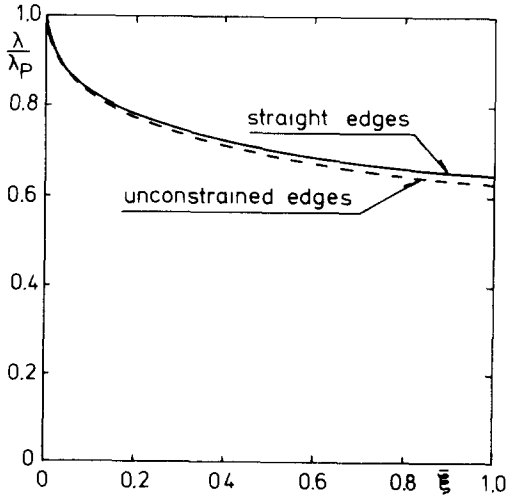

Fig. 6. Collapse load vs imperfection amplitude for elastic–plastic plate without creep ($h/b = 0.035$, $a/b = 1$, $\nu = 0.3$, $\sigma_Y/E = 0.00337$, $m = 10$)

The creep buckling in Fig. 5 due to the instability condition (4.5) is clearly a result of reaching a state corresponding to a limit point instability for the elastic–plastic structure. Similarly, creep buckling may occur instantaneously by reaching a bifurcation point with unstable post-buckling behaviour, as has been discussed by Obrecht[19] for the case of a circular cylindrical shell under axial compression. Thus, the type of creep buckling to be expected for a given structure may be judged by considering the post-buckling behaviour and the imperfection-sensitivity without creep[20].

In Fig. 7 results are compared for various levels of yield stress in plates with the same initial imperfection $\bar{\xi} = 0.1$. Only the constrained in-plane boundary conditions are considered, and here the smaller aspect ratio $a/b = 0.8$ is chosen, for which a higher creep rate is predicted in Fig. 3. As a reference the yield stress used in Fig. 5 is denoted by σ_{y0}. Now, for $\sigma_y = \sigma_{y0}$ yielding has started already at $t = 0$, and creep buckling occurs a little faster than for the square plate in Fig. 5, at $w_{max}/h \approx 1$. This earlier failure is partly dependent on the fact that the plastic buckling load λ_P is slightly smaller for $a/b = 0.8$, so that here $\lambda/\lambda_R = 0.65$ corresponds to $\lambda/\lambda_P = 0.732$. For $\sigma_y/\sigma_{y0} = 1.5$ creep buckling occurs considerably later, rather shortly after initial yielding and still at a small deflection $w_{max}/h \approx 3$. In this case bifurcation of the perfect plate occurs in the elastic range considerably below the yield stress. For $\sigma_y/\sigma_{y0} = 2$ little difference is found from the behaviour of an elastic plate, even though yielding starts at $w_{max}/h \approx 2$. Clearly, a low yield stress reduces the failure time t_F considerably; but for higher yield stresses, where yielding starts late in the process, the failure time is rather insensitive to the value of σ_y.

In Fig. 8 the computations of Fig. 7 are repeated with the one difference that now the strain hardening exponent is taken to be $m = 3$. Here, the failure time for $\sigma_y = \sigma_{y0}$ differs rather little from the value of t_F predicted by the elastic analysis, and for $\sigma_y/\sigma_{y0} = 1.5$ the failure time is even a little larger than that predicted by elasticity. Thus, the strong sensitivity to σ_y found for $m = 10$ is not present for the high hardening material considered here. This difference is related to the fact that an elastic–plastic plate without creep is imperfection-sensitive for $m = 10$, as shown in Fig. 6, but not for $m = 3$[16]. The result found for $\sigma_y/\sigma_{y0} = 1.5$ that plasticity slightly decreases the rate of creep buckling may be explained by the smaller peak values of stresses, when plasticity is accounted for, which leads to smaller rates of creep straining.

In the paper of Mathauser and Deveikis[11] a number of compressive stress–strain curves are shown for the aluminium–alloy sheet investigated. These curves show the well known decrease of σ_y for increasing temperature, but they also show that for a given temperature the yield stress decreases with increasing exposure time. In an attempt to model this type of behaviour a few computations have been made for a time dependent σ_y, still based on the

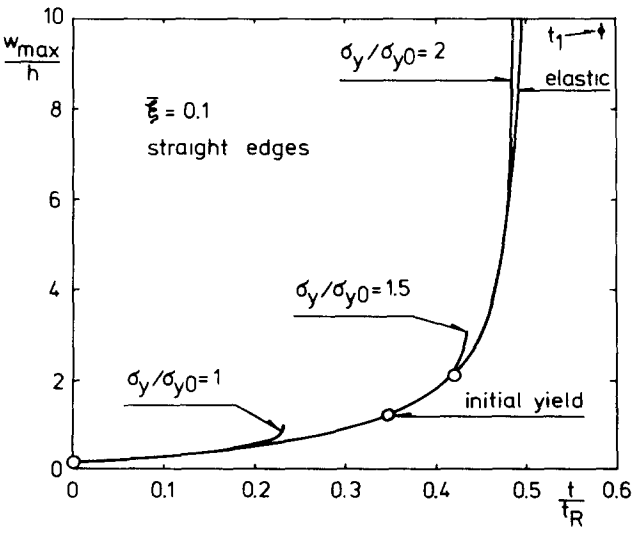

Fig. 7. Maximum deflection vs time for elastic-plastic plate subject to creep buckling ($h/b = 0.035$, $a/b = 0.8$, $\nu = 0.3$, $n = 6$, $\sigma_{y0}/E = 0.00337$, $m = 10$, $\lambda/\lambda_R = 0.65$).

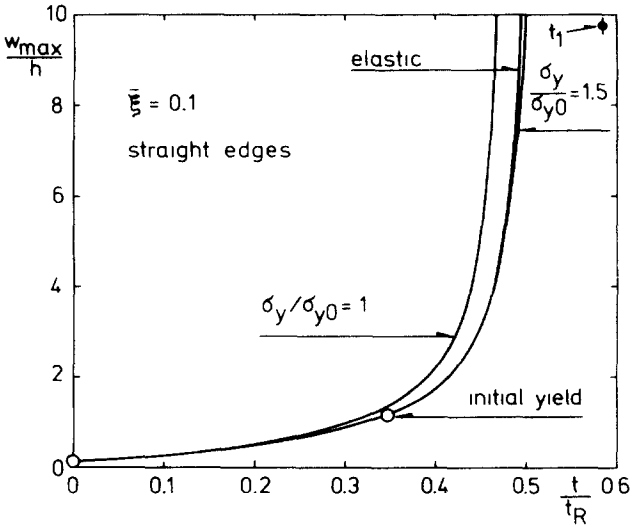

Fig. 8. Maximum deflection vs time for elastic-plastic plate subject to creep buckling ($h/b = 0.035$, $a/b = 0.8$, $\nu = 0.3$, $n = 6$, $\sigma_{y0}/E = 0.00337$, $m = 3$, $\lambda/\lambda_R = 0.65$)

simplifying assumption that plastic yielding and creep are independent processes. Led by the experimental results[11] the time dependence is taken to be of the form

$$\sigma_y = \sigma_{y0}\left\{1 - \gamma_1 \ln\left(1 + \gamma_2 \frac{t}{t_R}\right)\right\}. \tag{4.7}$$

The results shown in Fig. 9 are obtained for $\gamma_2 = 100$ and $\gamma_1 = 0.1083$, so that σ_y is halved at $t/t_R = 1$, and for $\sigma_{y0}/E = 0.00674$. For the small imperfection $\bar{\xi} = 0.02$ the behaviour is much like that found in Fig. 5, even though with (4.7) yielding starts late. However, for $\bar{\xi} = 0.5$ creep buckling occurs so fast that σ_y is still rather large, and thus the failure time t_F is more like that found in Fig. 2.

Finally, a few computations have been made for comparison with the experiments of Benoit and Hoff[12]. These experiments were made with square, thinwalled box columns, to approximate the boundary conditions (2.17)–(2.19), (2.21) and (2.22). The material used was 2024-T3 aluminium alloy sheet with geometry given by $b = 0.0381$ m and $h/b = 0.01333$. At the test temperature 315.6°C the Young's modulus was $E = 4.96 \times 10^{10}$ N/m^2 and the values of the creep constants in (2.4) were $n = 6$ and $k = 3.16 \times 10^{-48}$ hr^{-1} (N/m^2)$^{-6}$. For six tests at a load level corresponding to $\lambda/\lambda_R = 0.532$ the average failure time was 11.7 hr. The corresponding reference time (2.27) is $t_R = 8.55$ hr, and the failure times computed in Fig. 10, accounting only for creep and elasticity, are $t_F = 5.7$ hr for $\bar{\xi} = 0.1$ and $t_F = 11.3$ hr for $\bar{\xi} = 0.02$. Here the wavelength $a/b = 0.8$ has been chosen, at which the rate of creep buckling is relatively high

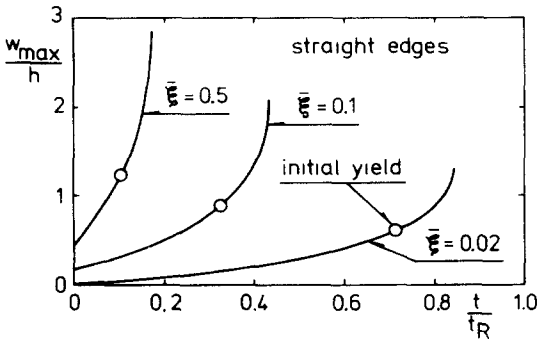

Fig. 9. Maximum deflection vs time for elastic-plastic plate subject to creep buckling, with a time dependent yield stress ($h/b = 0.035$, $a/b = 1$, $\nu = 0.3$, $n = 6$, $\sigma_{y0}/E = 0.00674$, $m = 3$, $\gamma_1 = 0.1083$, $\gamma_2 = 100$, $\lambda/\lambda_R = 0.65$).

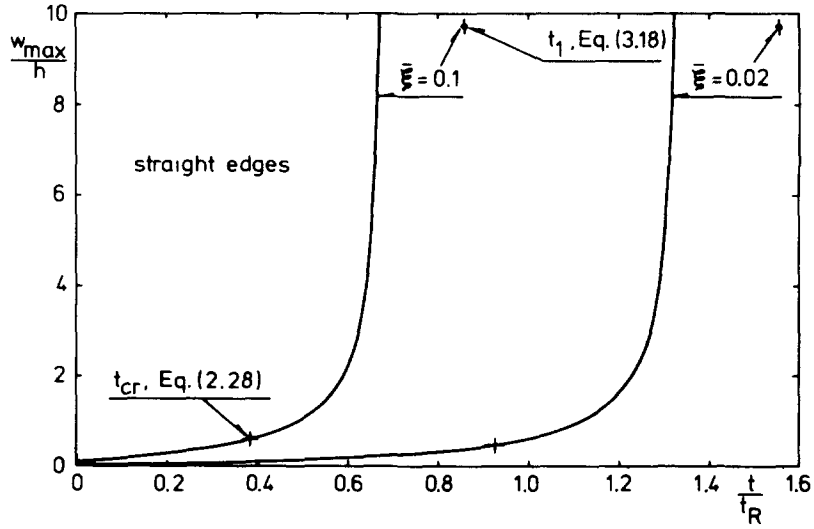

Fig. 10. Maximum deflection vs time for elastic plate subject to creep buckling ($h/b = 0.01333$, $a/b = 0.8$, $\nu = 0.3$, $n = 6$, $\lambda/\lambda_R = 0.532$).

according to Fig. 3. Before the tests the maximum initial deviation from flatness Δ was measured using a sliding micrometer, and for the six tests considered $\Delta/h \approx 0.3$–0.6 was found. This however is not directly a measure of the imperfection amplitude $\bar{\xi}$, as neither the wavelength nor the general shape of the initial deviations from flatness are known. The failure times predicted in Fig. 10 agree reasonably with the experimental results, if the part of the imperfection in the shape of the bifurcation mode (2.23) has a rather small amplitude $\bar{\xi} \approx 0.02$.

5. CONCLUSIONS

The investigation of creep buckling for rectangular plates under axial compression has shown a strong dependence on the material nonlinearities. The rate of creep buckling is very dependent on the temperature, due to the temperature dependence of the creep coefficient in Norton's law, and on the stress level due to this power law, as is well known. However, the creep exponent also has the qualitative effect that the failure time is quite imperfection-sensitive for a high creep exponent, whereas for a smaller creep exponent this sensitivity is much reduced.

When plastic yielding also occurs, in addition to elastic and creep deformations, the imperfection-sensitivity is considerably increased, and for sufficiently large imperfections the creep lifetime may vanish. For a low hardening material the plasticity also results in instantaneous collapse at a rather small buckling deflection, whereas for a more high hardening material creep buckling is merely characterized by deflections growing rapidly to large values, as in the case of elastic plates. This different behaviour at creep buckling is directly related to the post-buckling behaviour of the plates without creep.

An asymptotic analysis of the initial creep buckling behaviour has led to a simple time estimate that may be useful as an indication of the failure time.

REFERENCES

1 N. J. Hoff, Creep buckling of plates and shells. In *Proc. 13th Int. Cong. Appl. Mech.* (Edited by E. Becker and G. K. Mikhailov), pp. 124–140. Springer Verlag, New York (1973).
2. N. J. Hoff, Theory and experiment in the creep buckling of plates and shells. In *Buckling of Structures* (Edited by B. Budiansky), pp. 67–77. Springer Verlag, New York (1976).
3. L. Å. Samuelson, Creep buckling of a cylindrical shell under non-uniform external loads. *Int. J. Solids Structures* **6**, 91–116 (1970).
4. M. Życzkowski, Geometrically non-linear creep buckling of bars. In *Creep in Structures* (Edited by N. J. Hoff), pp. 307–325. Springer Verlag, New York (1962).
5. N. C. Huang, Creep buckling of imperfect columns. *J. Appl. Mech.* **43**, 131–136 (1976).
6. M. Życzkowski and A. Zaborski, Creep rupture phenomena in creep buckling. In *Mechanics of Viscò-Elastic Media and Bodies* (Edited by J. Hult), pp. 283–290. Springer Verlag, New York (1975).
7. G. N. Rabotnov and S. A. Shesterikov, Creep stability of columns and plates. *J. Mech. Phys. Solids* **6**, 27–34 (1957).

8. N J. Hoff, Creep buckling of rectangular plates under uniaxial compression. In *Engineering Plasticity* (Edited by J Heyman and F. A. Leckie), pp. 257–276. Cambridge University Press (1968).
9. N. J. Hoff, L. Berke, T. C. Honikman and I. M. Levi, Creep buckling of flat rectangular plates when the creep exponent ranges from 3 to 7. In *Advances in Creep Design* (Edited by A. I. Smith and A. M. Nicolson), pp. 421–441 Applied Science, London (1971).
10. I. M. Levi and N. J. Hoff, The postcritical behaviour of compressed plates that creep. *Ingenieur-Archiv* **38**, 329–342 (1969).
11. E. E. Mathauser and W. D. Deveikis, Investigation of the compressive strength and creep lifetime of 2024-T3 aluminum-alloy plates at elevated temperatures. *NACA Rep.* 1308 (1957).
12. M. Benoit and N. J. Hoff, Creep buckling of flat plates. Stanford University Department of Aeronautics and Astranautics Report SUDAAR No. 461 (1973).
13. F. K. G. Odqvist, Non-linear solid mechanics, past, present and future. In *Proc. 12th Int. Congr. Appl Mech.* (Edited by M. Hetényi and W. G. Wincenti), pp. 77–99. Springer Verlag, New York (1969).
14. J. W. Hutchinson and H. Obrecht, Tensile instabilities in strain-rate dependent materials. In *Proc. 4th Int. Conf on Fracture*, Vol. 1, pp. 101. Waterloo, Canada (1977).
15. N. Jones and P. F. Sullivan, On the creep buckling of a long cylindrical shell. *Int. J. Mech. Sci.* **18**, 209–213 (1976).
16. A. Needleman and V. Tvergaard, An analysis of the imperfection sensitivity of square elastic–plastic plates under axial compression. *Int. J. Solids Structures* **12**, 185–201 (1976).
17. D. Bushnell, Large deflection elastic–plastic creep analysis of axisymmetric shells. In *Numerical Solution of Nonlinear Structural Problems* (Edited by R. F. Hartung), Vol. 6, pp. 103–138. AMD/ASME, New York (1973).
18. J. L. Sanders, H. G. McComb and F. R. Schlechte, A variational theorem for creep with applications to plates and columns. *NACA Rep.* 1342 (1958).
19. H. Obrecht, Creep buckling and postbuckling of circular cylindrical shells under axial compression. *Int. J. Solids Structures* **13**, 337–355 (1977).
20. V. Tvergaard, Buckling behaviour of plate and shell structures. In *Proc. 14th Int. Cong. Theor. and Appl. Mech* (Edited by W. T. Koiter), pp. 233–247. North-Holland, Amsterdam (1976).